$\boldsymbol{k}+\boldsymbol{H}+\boldsymbol{q}$ and $\boldsymbol{k}+\boldsymbol{H}+\boldsymbol{q}'$ beams may not. In the terminology of the local reciprocal lattice, this statement implies that the two-beams, $\boldsymbol{k}$ and $\boldsymbol{k}+\boldsymbol{H}(r)$, are considered to be under dynamical diffraction (see Paper II).

Here we apply the two-wave approximation with the understanding described above. The canonical transformation of interest then functions only to diagonalize the matrix $\mathbf{K}$ with respect to $\boldsymbol{q}$ and $\boldsymbol{q}'$ defined in Section 2, not with respect to $\boldsymbol{I}$ and $\boldsymbol{J}$. From this point on, the subscripts q on W in (3.2) really become identical to the q's defined in Section 2. Equation (3.3) then gives a set of equations for the $\boldsymbol{O}$ and $\boldsymbol{H}$ beams just as for a perfect crystal. The Hamilton-Jacobi Eq. (3.5 b) now takes the form of the well-known dispersion equation for the two-wave case. Using the Hamiltonian defined by this equation, we can derive Hamilton's canonical equation in the two-wave approximation. This equation gives the "relativistic" equation for the rays as Kato [2] and Kambe [4] derived previously.

[1] P. Penning and D. Polder, Philips Res. Rep. **16**, 419 [1961].
[2] N. Kato, J. Phys. Soc. Japan **18**, 1785 [1963]; **19**, 67, 971 [1964].
[3] U. Bonse, Z. Phys. **177**, 385 [1964].
[4] K. Kambe, Z. Naturforsch. **20 a**, 770 [1965]; **23 a**, 25 [1968].
[5] S. Takagi, Acta Cryst. **15**, 1311 [1962]; J. Phys. Soc. Japan **26**, 1239 [1969].
[6] D. Taupin, Bull. Soc. Franc. Mineral Crist. **87**, 469 [1964].
[7] M. Ashkin and M. Kuriyama, J. Phys. Soc. Japan **21**, 1549 [1966]; M. Kuriyama and T. Miyakawa, J. Appl. Phys. **40**, 1697 [1969]; Acta Cryst. **A 26**, 667 [1970]; M. Kuriyama, J. Phys. Soc. Japan **23**, 1369 [1967]; **25**, 846 [1968]; Phys. Stat. Sol. **24**, 743 [1967]; Acta Cryst. **A 25**, 682 [1969].
[8] M. Kuriyama, Acta Cryst. **A 26**, 56 [1970] (referred to as Paper I); Acta Cryst. **A 28**, 588 [1972] (referred to as Paper II).
[9] M. Kuriyama, Acta Cryst. **A 27**, 634 [1971].

A Comparison of Diffuse Scattering by Defects Measured in Anomalous Transmission and Near Bragg Reflections *

Bennett C. Larson and F. W. Young, Jr.

Solid State Division, Oak Ridge National Laboratory, Oak Ridge, Tennessee 37830

(Z. Naturforsch. **28 a**, 626–632 [1973]; received 21 February 1973)

Dedicated to Prof. Dr. G. Borrmann on the occasion of his 65th birthday

The diffuse scattering from neutron-irradiation-produced defects in copper was measured in anomalous transmission and near the 111 Bragg reflection. The results were related through the theory of Dederichs, and the intensities and forms of the scattering curves obtained from the two measurements were found to be in good agreement over a wide range of defect concentrations and sizes. It was shown that the intercept of a plot of the diffuse scattering intensity $I^s(q_0)$ vs $\ln(q_0)$ is at $q_0 = e^{1/2}/R$ for defects of uniform radius R and at $q_0 \cong 1/R_0\, e$ for an exponential size distribution of average size R_0.

Introduction

One of the consequences of the discovery of the anomalous (Borrmann) transmission of X-rays through nearly perfect crystals has been a renewed interest in the use of X-ray scattering for the investigation of defects in crystals. The decrease in anomalous transmission resulting from defects has been studied for impurities in silicon [1] and germanium [2], for defect clusters produced by neutron irradiation in copper [3], and for interstitials in copper [4]. This decrease in transmission results from the lattice strains introduced by the defects and the theory for describing this effect has been developed by Dederichs [5], and we [6] have shown the theory to be phenomenologically correct for neutron irradiated copper. The decrease in anomalous transmission is described in terms of an effective absorption coefficient μ^* which is the sum of two components, μ_{PE} due to enhanced photoelectric absorp-

* Research sponsored by the U.S. Atomic Energy Commission under contract with Union Carbide Corporation.

Reprint requests to F. W. Young, Jr., Solid State Division, Oak Ridge National Laboratory, Post Office Box X, *Oak Ridge, Tenn. 37830*, U.S.A.

tion at the atoms which are distorted from lattice positions, and μ_{DS} due to the waves which are diffusely scattered from the dynamical wave and hence absorbed in the crystal. Also, there is diffuse scattering near reflections in the Bragg geometry which is caused by the defects [7, 8]. From the theories this diffuse scattering [9] and μ_{DS} of anomalous transmission [5] are related. For this paper we have measured both anomalous transmission and diffuse scattering on copper crystals which had been neutron irradiated and compared these values through the theory.

Theory

In the theoretical treatment of the effect of clustered defects on anomalous transmission given by Dederichs [5] the decrease in transmitted intensity is represented in terms of an effective absorption coefficient μ^* such that the ratio of the integrated Borrmann intensities for crystals containing defects R_{def} to that for a perfect crystal R_{per} is given by

$$R_{def}/R_{per} = e^{-\mu^* t} \tag{1}$$

where t is the effective thickness of the crystal. $\mu^* = \mu_{PE} + \mu_{DS}$ has two components, μ_{PE} related to the absorption caused by atoms displaced by the strain fields around defects and μ_{DS} arising from X-rays scattered out of the anomalously transmitted beam by Huang diffuse scattering generated by the strain fields.

Considering a concentration of dislocation loops C_L (loops/atom) with radius R and Burgers vector b, μ_{DS} for a reflection of reciprocal lattice vector h is given by [5]

$$\mu_{DS} = \frac{r_0^2}{V_c}\left(f e^{-M}\frac{h}{k}\right)^2 C_L\left(\frac{b\pi R^2}{V_c}\right)^2 \ln(q_L/q_c)\left(\frac{8\pi}{15}+\frac{\pi}{15}\frac{(-1+6\nu+3\nu^2)\cos^2\Theta_B}{(1-\nu)^2}\right) \tag{2}$$

where r_0 is the classical electron radius, V_c is an atomic volume, $f e^{-M}$ is the atomic scattering factor with Debye-Waller factor e^{-M}, $k = 2\pi/\lambda$ where λ is the X-ray wavelength, $q_c = 4\pi r_0 f e^{-M}/V_c h$ is a reciprocal extinction length [5] of the reflection, $q_L = 1/R$ and ν is Poisson's ratio. μ_{PE} is given approximately by

$$\mu_{PE} = \mu_0 e^{-M} L = \mu_0 e^{-M} C_L R^3 (h b)^{3/2}/2 V_c \tag{3}$$

where μ_0 is the linear photoelectric absorption coefficient and L is the static Debye-Waller factor associated with the strain fields of the defects.

The Huang diffuse scattering near Bragg reflections (also thin crystal Laue reflections) measured with a wide open detector, as shown in Fig. 1, is closely related to that associated with μ_{DS} in the Borrmann case. Dederichs [9] has considered this "integral" diffuse scattering which is characterized by a minimum q-vector $q_0 = h(\Delta\Theta)\cos\Theta_B$ when the sample is set at an angle $\Delta\Theta$ off the Bragg angle Θ_B. The diffuse intensity is calculated by considering contributions from all q's having components q_0 perpendicular to the Ewald sphere (considered as a tangent plane here) and integrating over components q' in the tangent plane such that $q = (q_0^2 + q'^2)^{1/2}$. This intensity is asymmetrical; however, the symmetrical part of this intensity

$$I^s(q_0) = \tfrac{1}{2}\left(I(q_0) + I(-q_0)\right) \tag{4}$$

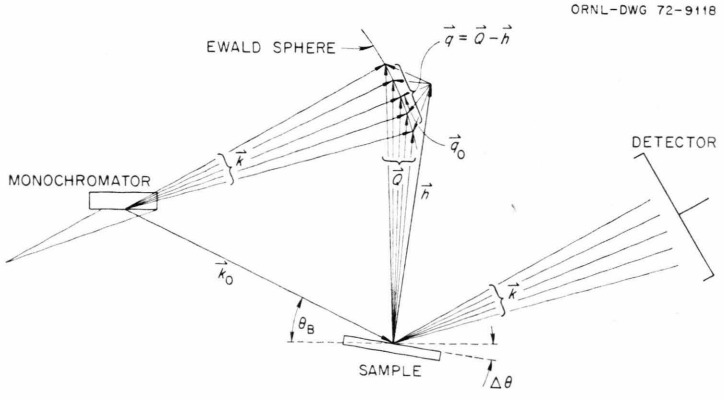

Fig. 1. Schematic drawing of the scattering geometry for "integral" diffuse scattering using a Bragg monochromator showing the incident beam k_0, and the scattered X-rays k.

has been shown [9] to be of the form

$$I^s(q_0) \sim C_L (b\pi R^2/V_c)^2 \ln(q_L/q_0) \qquad (5)$$

for $q_0 \ll q_L$. The above expression and the expression for μ_{DS} were obtained neglecting the contribution from $q \geqq q_L = 1/R$ which characterizes the end of the Huang scattering which has the well-known q^{-2} scattering law.

For $q_0 \ll q_L$ and in the anomalous transmission case the scattering from $q \gtrsim q_L$ is not too significant; however, for $q_0 \gtrsim q_L$ this is not the case so we have considered the contribution from $q \geqq q_L$ by approximating the scattering with a q^{-4} dependence for $q \geqq q_L$ and joining to the q^{-2} dependence at $q = q_L$. The integral over q' in the tangent plane now has the form

$$\int_0^{\sqrt{q_L^2 - q_0^2}} \frac{q'\,dq'}{q_0^2 + q'^2} + \int_{\sqrt{q_L^2 - q_0^2}}^{q_M} \frac{q_L^2\, q'\,dq'}{(q_0^2 + q'^2)^2} \quad (q_0 \leqq q_L) \qquad \text{and} \qquad \int_0^{q_M} \frac{q_L^2\, q'\,dq'}{(q_0^2 + q'^2)^2} \quad (q_0 \geqq q_L). \qquad (6)$$

The upper limit q_M is rather indefinite, but since it is much larger thant q_0 it has been considered infinite in evaluating the integrals. These integrations lead to the result that $\ln(q_L/q_c)$ in Eq. (2) is replaced by $\ln(q_L/q_c) + 1/2 = \ln(q_L e^{1/2}/q_c)$ and $\ln(q_L/q_0)$ in Eq. (5) is replaced by $\ln(q_L e^{1/2}/q_0)$ if $(q_0 \leqq q_L)$ and $q_L^2/2\, q_0^2$ if $q_0 \geqq q_L$.

In analogy with Eq. (2) and as suggested by Dederichs [5] it is possible to include both Eqs. (2) and (5) in a single expression if we write the integral diffuse scattering cross section in the form of a linear scattering cross section $\mu_{DS}(q_0)$. That is

$$\mu_{DS}(q_0) = \frac{r_0^2}{V_c}\left(\frac{f e^{-M} h}{k}\right)^2 C_L \left(\frac{b\pi R^2}{V_c}\right)^2 F(q_L/q_0) \left(\frac{8\pi}{15} + \frac{\pi}{15}\,\frac{(-1 + 6\nu + 3\nu^2)\cos^2\Theta_B}{(1-\nu)^2}\right) \qquad (7)$$

with

$$F(q_L/q_0) = \ln(q_L e^{1/2}/q_0) \quad (q_0 \leqq q_L), \qquad F(q_L/q_0) = q_L^2/2\, q_0^2 \quad (q_0 \geqq q_L) \qquad (8)$$

where $\mu_{DS}(q_c) \equiv \mu_{DS}$ for anomalous transmission, and $\mu_{DS}(q_0) \equiv \mu_{DS}$ for the Bragg or thin crystal Laue cases. A plot of $I^s(q_0)$ vs $\ln(q_0)$ for small q_0 therefore leads to a straight line with intercept at $q_0 = q_L e^{1/2}$ and for large q_0 a plot of $\ln[I^s(q_0)]$ vs $\ln(q_0)$ has a slope of -2.

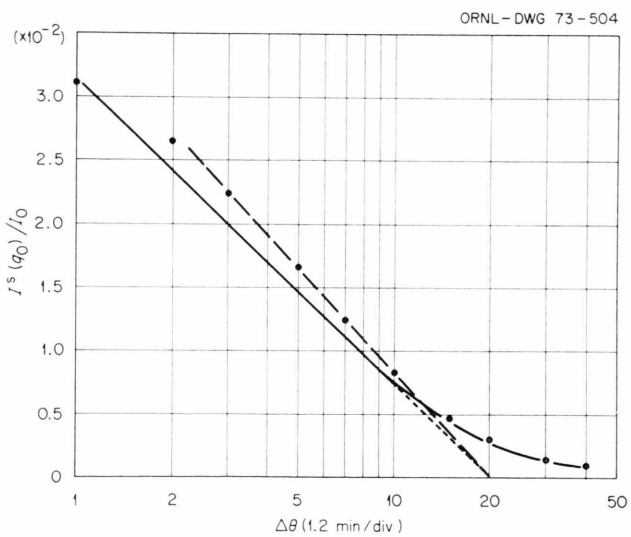

Fig. 2. Integral diffuse scattering vs $\ln(\Delta\Theta)$ for a dose of 10.8×10^{18} n/cm^2. The coarse dashed line drawn through the experimental points defines the intercept and the solid line is the computed curve for an exponential distribution with $R_0 = 18.5$ Å ($q_5 = 9.88 \times 10^{-4}$ Å^{-1}/div).

In this form μ_{DS} obtained from anomalous transmission measurements can be directly compared with the measured diffuse scattering in Bragg or Laue cases given by

$$\frac{I^s(q_0)}{I_0} = \frac{\mu_{DS}(q_0)}{2\,\mu_0} \quad \text{symmetrical Bragg}$$
$$\frac{I^s(q_0)}{I_0} = \mu_{DS}(q_0)\, t\, e^{-\mu_0 t} \quad \text{symmetrical Laue} \qquad (9)$$

where I_0 is the incident beam intensity and $t = t_0/\cos\Theta_B$ (t_0 = perpendicular thickness of the sample).

When a distribution of sizes is to be considered rather than defects all of the same size, the interpretation of these formulae becomes somewhat more difficult and their application to experimental measurements must be considered in conjunction with the size distribution.

In particular for a distribution $C_L(R_i)$, $\mu_{DS}(q_0)$ has the form

$$\mu_{DS}(q_0) \sim \sum_i C_L(R_i)\, R_i^4 \ln(e^{1/2}/q_0 R_i) \qquad (10)$$

for q_0 much less than those q_L associated with the largest R_i, and

$$\mu_{DS}(q_0) \sim \sum C_L(R_i)\, R_i^2/2\, q_0^2 \qquad (11)$$

for large q_0 (q_L has been replaced by $1/R_i$). $\mu_{DS}(q_0)$ for small q_0 weights the sizes similar to a fourth moment while for large q_0, $\mu_{DS}(q_0)$ represents a second moment sampling of the size distribution.

For an exponential distribution $C_L(R) = C_L(0)\, e^{-R/R_0}$ truncated at $R = R_M$, Eq. (10) can be written in integral form as

$$\mu_{DS}(q_0) \sim (C_L(0)/R_0) \int_0^{R_M} e^{-R/R_0} R^4 \ln(e^{1/2}/q_0 R)\, dR. \qquad (12)$$

This expression is apparently not intergrable in closed form for finite R_M; however, for $1/q_0 \gg 5\, R_0$, it appears that R_M can be taken as infinity without introducing serious error. The integral can then be performed [10] giving

$$\mu_{DS}(q_0) \sim 24\, C_L(0) R_0^4 \left(\ln(e^{1/2}/q_0 R_0) + C_E - \tfrac{25}{12}\right). \qquad (13)$$

$C_E = 0.5772$ is Eulers constant. This can be written approximately as

$$\mu_{DS}(q_0) \sim 24\, C_L(0)\, R_0^4 \ln(1/q_0 R_0 e) \quad q_0 \ll 1/5\, R_0 \qquad (14)$$

which leads to an intercept at $q_0 \cong 1/R_0\, e$ in a plot of $I^s(q_0)$ versus $\ln(q_0)$.

Experimental

The copper crystals used in this experiment were lamellae with (111) faces and dimensions $1 \times 1 \times t_0$ cm, $0.025 < t_0 < 0.1$. These crystals had dislocation densities $\sim 10^2/\text{cm}^2$ and were shown to be essentially perfect from the standpoint of integrated Borrmann and Bragg intensities before irradiation. The irradiations at room temperature to doses of $3.6 - 10.8 \times 10^{18}$ n/cm^2 ($E > 0.6$ MeV) have been described earlier [6], and the 1×10^{18} irradiation dose was performed in the same facility. The 8 °K irradiation was carried out in the CP-5 reactor at Argonne National Laboratory in a fission spectrum to a dose of 1.3×10^{18} n/cm^2 by T. H. Blewitt.

The integrated-anomalous-transmission measurements were carried out on a double-crystal diffractometer using a Bragg monochromator and the diffuse scattering measurements were made on the same instrument using both Bragg and Borrmann monochromator geometries, the Borrmann monochromator reducing the background in measurements near the Bragg reflection and eliminating the π (parallel) polarized X-rays. Diffuse scattering measurements were made for both positive and negative deviations from the Bragg angle and the background correction due to the tails of the Bragg reflection, thermal diffuse scattering and Compton scattering was obtained by making similar measurements on unirradiated crystals. The detector subtended a cone accepting X-rays scattered $\pm 5°$ from the angle of the Bragg reflection which was sufficient to collect all the scattering from the defect clusters.

Results

The results of the anomalous transmission measurements on the 111 reflection of the irradiated crystals for CuKα and MoKα X-rays are tabulated in the form of μ^* values in Table 1. The separation of μ^* into μ_{PE} and μ_{DS} was carried out [6] by satisfying the wavelength dependence of the two components as given in Eq. (2) and Eq. (3), with the constraint that the sum be the measured μ^*.

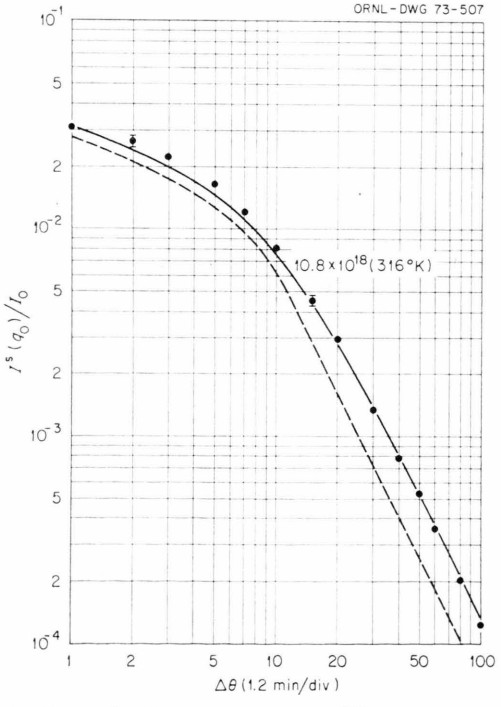

Fig. 3. Integral diffuse scattering vs $\Delta\Theta$ ($q_0 = 9.88 \times 10^{-4}$ Å^{-1}/div) for a neutron dose of 10.8×10^{18} n/cm^2 at 316 K. The points are experimental. The solid line was computed for an exponential distribution with $R_0 = 18.5$ Å and the dashed line for defects of uniform size $R = 84$ Å.

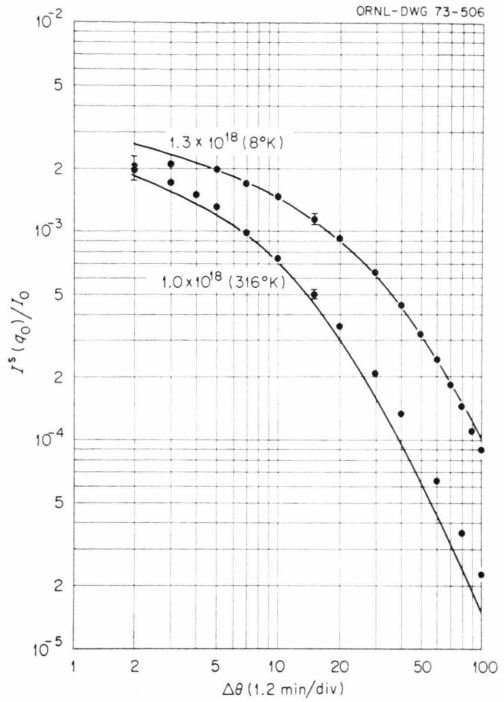

Fig. 4. Integral diffuse scattering vs $\Delta\Theta$ for neutron doses of 1.3×10^{18} n/cm² at 8 K and 1.0×10^{18} n/cm² at 316 K, resp. The solid lines were calculated for exponential distributions with $R_0 = 5.3$ Å for the upper curve and $R_0 = 14.5$ Å for the lower curve.

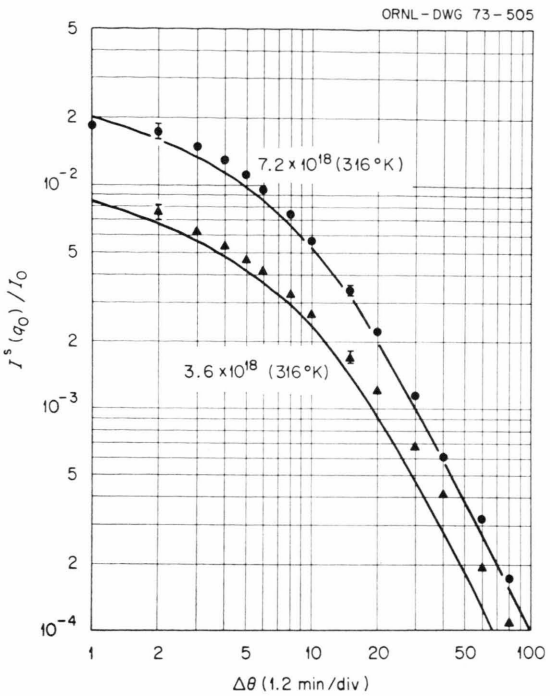

Fig. 5. Integral diffuse scattering vs $\Delta\Theta$ for neutron doses of 7.2×10^{18} n/cm² and 3.6×10^{18} n/cm², resp., at 316 K. The lines were calculated for $R_0 = 17$ Å for the upper curve and $R_0 = 16$ Å for the lower curve.

The integral diffuse scattering measurements, made near the 111 Bragg reflection using CuKα radiation, are presented in terms of the ratio of the diffuse scattering intensity to the incident beam intensity in Figs. 2, 3, 4 and 5. The individual points are the measured values as obtained using a Borrmann monochromator; measurements made with a Bragg monochromator were about 20% smaller, as expected from polarization corrections, but the shapes of the curves were equivalent. Figure 2 contains a plot of the integral scattering intensity versus $\ln q_0$ for a neutron dose of 10.8×10^{18} n/cm², irradiation temperature 316 °K. Similar plots were made for the other doses, yielding measurements of the intercept in each case. This intercept is inversely related to the characteristic size of the defect clusters. Thus, it is possible to identify qualitatively a trend toward increasing defect cluster sizes for increasing irradiation doses and irradiation temperatures from the intercept values listed in Table 1.

Table I. Diffuse Scattering Parameters.

Dose	λ	μ^*	μ_{DS}	μ_{PE}	Intercept	R_0
1.3×10^{18} n/cm²	CuKα	12.9 cm^{-1}	3.6 cm^{-1}	9.3 cm^{-1}	6.9×10^{-2} Å^{-1}	5.3 Å
	MoKα	10.1	1.0	9.1		
1.0	CuKα	6.2	2.9	3.3	2.50	14.5
	MoKα	4.0	0.8	3.2		
3.6	CuKα	23	10.7	12.3	2.26	16
	MoKα	15	3.0	12.0		
7.2	CuKα	49	25.6	23.4	2.13	17
	MoKα	30	7.0	23.0		
10.8	CuKα	75	39.0	36.0	1.97	18.5
	MoKα	46	10.8	35.2		

The values of μ_{DS} from anomalous transmission can be compared with the intensities measured in the Bragg geometry by utilizing the q_0 dependence of the diffuse scattering given in Eq. (7):

$$\frac{I^s(q_0)}{I_0} = \frac{\mu_{DS}}{2\mu_0}\frac{F(q_L/q_0)}{F(q_L/q_c)}. \quad (15)$$

Thus the integral diffuse scattering is related to the μ_{DS} from the anomalous transmission multiplied by the "form factor" $(F(q_L//q_0))/(F(q_L/q_c))$.

The dashed curve in Fig. 3 was calculated in this manner for an intercept of 1.97×10^{-2} Å^{-1} obtained from Fig. 2 and $\mu_{DS}=39$ cm^{-1} taken from Table 1. Of course this calculation assumes all of the loops to be of the same size, $R=e^{1/2}/1.97\times10^{-2}=84$ Å. A more reasonable assumption for neutron irradiated copper[11] is an exponential distribution defined by $C_L(R)=C_L(0)\,e^{-R/R_0}/R_0$ where R_0 characterizes the average size in the distribution. From Eqs. (10 – 12) the effect of this distribution of sizes can be taken into account by replacing Eq. (15) by

$$\frac{I^s(q_0)}{I_0} = \frac{\mu_{DS}}{2\mu_0}\frac{\sum_i e^{-R_i/R_0}R_i^4 F(1/q_0R_i)}{\sum_i e^{-R_i/R_0}R_i^4 F(1/q_cR_i)}. \quad (16)$$

The intercept of a plot of this function versus $\ln(q_0)$ for small q_0 is given approximately by $1/R_0\,e$ [see Eq. (14)]. Equation (16) has been evaluated numerically using an exponential size distribution with various R_0. Increments of R_i in the summation were taken as 1 Å and a maximum R_i of 400 Å was used for R_0 in the range 3 – 25 Å. It was then possible to choose the R_0 values required to obtain the measured intercepts, as demonstrated in Fig. 2, and these are listed in Table 1. R_0 values calculated using Eq. (14) are within 2% of those listed in Table 1. Using the values of μ_{DS} and R_0 from Table 1, the diffuse scattering intensities were calculated as a function of q_0 and the results are presented as the solid curves in Figures 2 – 5.

Discussion

The good agreement between the diffuse scattering as measured by anomalous transmission and that measured near Bragg reflections gives confidence that these processes are adequately accounted for by the theory. There are two aspects of this comparison, the magnitudes and the detailed shapes of the scattering curves. The magnitudes are derived from the experimental measurements of μ_{DS} and the shapes are determined by the "form factor" $(\mu_{DS}(q_0))/(\mu_{DS}(q_c))$. The agreement ($\sim10\%$) between the magnitudes is very good since there are no adjustable parameters. The smallest q_0 for which intensities were measured in these experiments was about five times q_c (the effective q_0 value for anomalous transmission) but for reasonable exponential distributions the "form factor" was insensitive to changes in R_0 for these q_0. For larger q_0 ($>10^{-2}$) the form factor becomes quite sensitive to changes in R_0. Thus, although overall the fit between the computed and experimental scattering curves is good, the small discrepancies between them are considered to be significant. The assumptions used in the computation are: 1) that the scattering curve could be approximated as q^{-2} for $q \leqq 1/R$ and q^{-4} for $q \geqq 1/R$, 2) any changes in the anisotropy factor in Eq. (7) as a function of q_0 could be neglected, and 3) an exponential size distribution of dislocation loops. Assumptions 1) and 2) are oversimplifications made to facilitate computation, but the "form factor" ratio $(\mu_{DS}(q_0))/(\mu_{DS}(q_c))$ tends to minimize their effects, especially for small q_0. The effect of a more realistic approximation to the scattering curve is being investigated further. The shape of the computed curves for small q_0 is rather insensitive to the size distribution used, but at larger q_0 the size distribution was found to be important, and it should be noted that an exponential distribution (observed in electron microscopy studies) produces a much better fit than does a single size (Figure 3). The effect of small deviations from an exponential distribution is being investigated in further detail and will probably lead to improved fits.

Since the best fits were obtained for the low temperature and the 10.8×10^{18} irradiations, those with the smallest and largest size distributions, it is clear that the experimental data can be fitted over this range of R_0. Therefore, the systematic variation in the fits with irradiation dose at 316 °K suggests a change in size distribution with dose. While such a change in size distribution has not been observed in electron microscopy studies, it is possible their experimental precision has not been sufficient to detect it.

It had been pointed out earlier [7] that the value of the intercept in a plot $I^s(q_0)$ vs $\ln(q_0)$ was related to the size of the loops. In the more complete development presented in this paper it was shown that this intercept is at $q_0 = e^{1/2}/R$ for defects of uniform radius R and at $q_0 \cong 1/R_0 e$ for an exponential size distribution. Hence the integral diffuse scattering measurements can be used to obtain quantitative measurements of loop sizes. From the electron microscopy studies, which indicate an exponential distribution, values for R_0 were obtained which are in approximate agreement with the values deduced from the present studies, Table 1.

Acknowledgement

We thank T. H. Blewitt for performing the low temperature irradiations.

[1] J. R. Patel and B. W. Battermann, J. Appl. Phys. **34**, 2716 [1963].
[2] O. N. Efimov and A. M. Elistratov, Soviet Phys. – Solid State **5**, 1364, 1543 [1964]; H. F. Wenzl, Z. Naturforsch. **26 a**, 495 [1971].
[3] T. O. Baldwin, F. A. Sherrill, and F. W. Young, Jr., J. Appl. Phys. **39**, 1541 [1968].
[4] L. S. Edelheit, J. C. North, J. G. Ring, J. S. Koehler, and F. W. Young, Jr., Phys. Rev. B **2**, 2913 [1970].
[5] P. H. Dederichs, Phys. Rev. B **1**, 1306 [1970].
[6] B. C. Larson and F. W. Young, Jr., Phys. Rev. B **4**, 1709 [1971].
[7] J. E. Thomas, T. O. Baldwin, and P. H. Dederichs, Phys. Rev. B **3**, 1167 [1971].
[8] P. Dederichs, J. Physics, F (in press, 1973).
[9] P. H. Dederichs, Phys. Rev. B **4**, 1041 [1971].
[10] D. B. deHaan, Nouvelles Tables d'Intégrales Définies, Hafner Publ. Co., New York 1957.
[11] M. Rühle, F. Häussermann, and M. Rapp, Phys. Stat. Sol. **39**, 609 [1970].

Use of Asymmetric Dynamical Diffraction of X-rays for Multiple-Crystal Arrangements of the $(n_1, +n_2)$ Setting

Kan Nakayama *, Hiroo Hashizume, Akio Miyoshi, Seishi Kikuta **, and Kazutake Kohra

Department of Applied Physics, Faculty of Engineering, University of Tokyo, Hongo, Bunkyo-ku, Tokyo

(Z. Naturforsch. **28 a**, 632–638 [1973]; received 1 February 1973)

Dedicated to Prof. Dr. G. Borrmann on the occasion of his 65th birthday

Asymmetric dynamical diffractions of X-rays are successively used for multiple crystals arranged in the $(n_1, +n_2)$ setting. Double successive asymetric diffractions of the $(n_1, +n_2)$ arrangement give a beam of peculiar spread in angle and wavelength. Triple successive asymmetric diffractions of the $(n, +n, -n)$ arrangement give a highly parallel and monochromatic beam for some appropriate combination of the asymmetry factors of the three crystals. Possible use of multiple asymmetric diffractions is discussed.

1. Introduction

Detailed information about dynamical diffraction phenomena of X-rays is obtained by using an incident beam of sufficiently narrow spread in angle and wavelength compared with the diffraction range of the crystal under investigation, which is of the order of seconds of arc. For such studies two kinds of arrangements are usually used: the double-crystal one of parallel or $(n, -n)$ setting and the triple-crystal one of $(n_1, +n_2, \pm n_3)$ setting.

In the former the spread of the beam used is narrow in angle only for each wavelength component, but, as a whole, not very narrow in angle nor wavelength. However, the dispersion effect due to the wavelength spread is eliminated owing to the parallel setting, in which the interplanar spacings of the diffracting planes of the first and second (specimen) crystals are equal to each other. In the parallel setting an extremely narrow angular spread of the incident beam is obtained by making use of the effects characteristic to dynamical diffraction

* Present address: National Research Laboratory of Metrology, *Kaga, Itabashi-ku, Tokyo.*

** Present address: The Institute of Industrial Science, University of Tokyo, *Roppongi, Minato-ku, Tokyo.*
Reprint requests to Dr. K. Kohra, University of Tokyo, Department of Applied Physics, Faculty of Engineering, *Bunkyo-ku, Tokyo 113*, Japan.